

SUPPLEMENTARY INFORMATION

Correlation Between Cationic Composition and Anionic Electrochemical Activity of Li_2MSeO Anti-perovskites

Mikhail V. Gorbunov, ^{*[a]} Oleg Janson, ^[a] Max Stöber, ^[a] Volodymyr Baran, ^[b] and Daria Mikhailova ^{*[a]}

[a] Dr. M. V. Gorbunov, Dr. D. Mikhailova, M. Stöber and Dr. O. Janson
Leibniz-Institut für Festkörper- und Werkstofforschung Dresden e. V.
Helmholtzstraße 20, 01069, Dresden, Germany
E-mail: m.gorbunov@ifw-dresden.de; d.mikhailova@ifw-dresden.de

[b] Dr. V. Baran
Deutsches-Elektronen Synchrotron DESY
Notkestraße 85, 22607, Hamburg, Germany

DFT Calculations

Density functional theory calculations were performed using the full-potential local-orbital code FPLO version 21^[37]. For the exchange-correlation potential, we used the generalized gradient approximation^[38]; the spin-orbit coupling was neglected. To check the stability of Li_2FeSeO , we considered all stoichiometric Li-, Fe-, Se- and O-containing materials from the Materials project^[39] and computed their GGA total energies using FPLO. To account for correlation effects in the Fe 3d shell in compounds containing iron and oxygen, we employed the DFT+U functional for total energy calculations. Following the literature^[40–41], we chose $U = 5$ eV and $J = 1$ eV as the interaction parameters and the fully localized limit as the double-counting correction. Correlation effects may be important also in Fe-containing compounds lacking oxygen. However, given the uncertainties in the choice of interaction parameters and general concerns in applying DFT+U to small-gap (or even conducting) materials, we refrain from using this computational scheme for such systems.

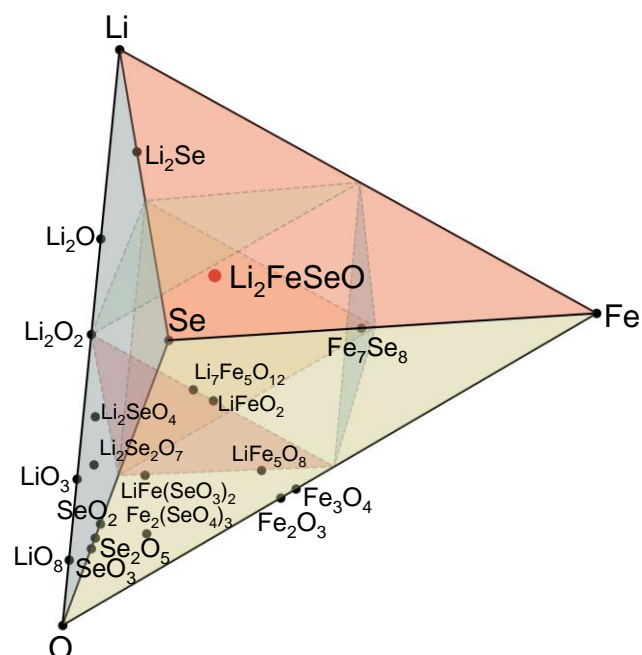


Figure S1. Thermodynamically stable compounds in the Li-Fe-Se-O system.

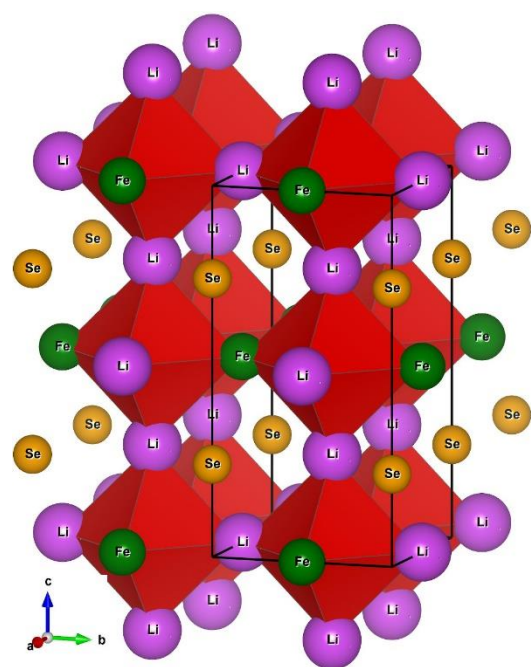


Figure S2. The lowest-energy configuration of disordered Li_2FeSeO .

Thermodynamically stable compositions were identified by convex hull calculations; entropy contributions were not considered. Following the work^[42], we shifted the total energies of oxygen and the oxygen-containing LiO_8 by 1.36 eV per O atom to account for GGA overbinding. After this correction, we arrived at 22 thermodynamically stable compounds in the Li-Fe-Se-O system (Figure S1).

To model the disordered structure of Li_2FeSeO , we considered the idealized anti-perovskite structure with the lattice parameter $a = 4.0196$ Å and doubled it along all three crystal axes. Next, we randomly distributed Li and Fe atoms over 24 cationic positions by keeping the Li:Fe=2:1 stoichiometry. From the resulting $24!/16!(24-16)! = 735471$ configurations, we removed all configurations with short-range Fe-Fe connections and all duplicate structures. Finally, we are left with 19 inequivalent configurations for which DFT+U total energies were calculated (for the ferromagnetic configuration). In this way, we found that the configuration with the lowest energy features (Fig. S2) features Fe-O chains running along the a axis (the b axis) at $z/c = 0$ ($z/c = 0.5$) has the lowest energy. (The same configuration was identified as the lowest-energy configuration for Li_2FeSO_8 .) All further calculations are done for this structural configuration.

The total energy of Li_2FeSeO lies 47 meV/atom above the convex hull; by projecting its composition onto the closest simplex of the convex hull, we found that it decomposes into Fe_7Se_8 , Fe, and Li_2O :



To compare the stability of Li_2FeSeO and Li_2FeSO , we added the total energies of Li_2FeSO , Li_2S and FeS, removed Se-containing compounds from the dataset, and repeated convex-hull calculations. In this way, we found that Li_2FeSO lies 150 meV/atom above the convex hull, and therefore is significantly less stable than Li_2FeSeO .

To calculate the densities of states (DOS), we considered the “chain” structural configuration, which for Li_2FeSeO has the lowest total energy. This configuration is described by the tetragonal $P4_2/mmc$ cell, with a single Wyckoff position for magnetic cations. To allow for antiferromagnetic solutions, we recast this structure into the orthorhombic $Pm\bar{m}m$ space group with a concomitant doubling along the c axis. For all three compounds – Li_2FeSeO , Li_2CoSeO , Li_2MnSeO – antiferromagnetic configurations have a lower total energy.

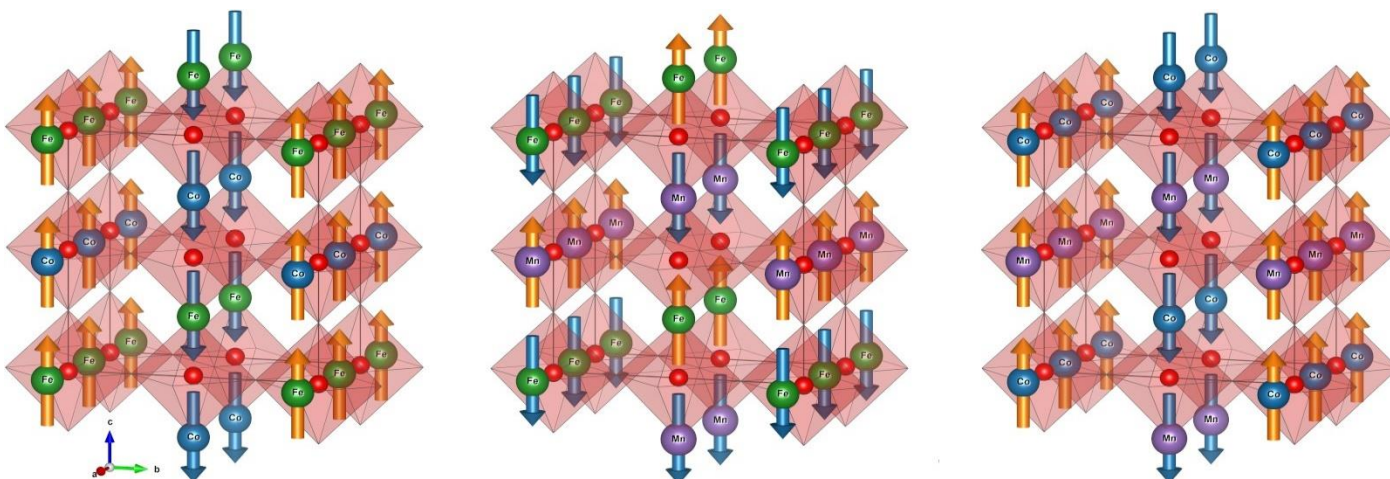


Figure S3. The lowest-energy magnetic configurations of (a) – $\text{Li}_2\text{Fe}_{0.5}\text{Co}_{0.5}\text{SeO}$, (b) – $\text{Li}_2\text{Fe}_{0.5}\text{Mn}_{0.5}\text{SeO}$, and (c) – $\text{Li}_2\text{Co}_{0.5}\text{Mn}_{0.5}\text{SeO}$.

To describe the mixed compositions with magnetic atoms A and B, we consider only one type of structural configuration in which magnetic atoms form A-O and B-O chains in one direction and A-O-B-O chains in the transverse direction. This configuration is described by relatively compact $Pmm2$ supercells featuring two inequivalent Wyckoff positions for each magnetic atom. By varying the initial spin polarizations of these four magnetic atoms, we can compute total energies of eight ($2^4/2 = 8$) inequivalent magnetic configurations. By comparing the total energies, we found that the antiferromagnetic configurations depicted in Fig. S3 have the lowest energy (note the difference between $\text{Li}_2\text{Fe}_{0.5}\text{Mn}_{0.5}\text{SeO}$ and the other two compounds).

Density of states (Fig. 3 in the main text) were calculated for the lowest-energy magnetic configurations. Dense k meshes with about 200 000 points per reciprocal atom were used.

Experimental Part

All the manipulations were done inside an Ar-filled glovebox (MBraun, Germany) with O_2 and H_2O concentrations not exceeding 0.5 ppm, except for preparation and heat treatment of the ampoules.

Synthesis and Powder X-ray Diffraction

Following reagents were used for the synthesis: Li_2O (Thermo Fisher Scientific, 99.5%), Fe, Co, (Sigma Aldrich, 99%), Mn (Merck, 99%), Se (Thermo Fisher Scientific, 99.5%). The powders were mixed in stoichiometric amounts (as described by reaction equation in the main text), to obtain 0.5 g of each desired material, and pressed into pellets (the applied pressure was 2 tons). Subsequently, the pellets were put into alumina crucibles and evacuated down to the pressure of $5 \cdot 10^{-5}$ mBar using the quartz tubes, to get rid of the residual moisture and air. Then they were partially refilled with argon up to 0.5 Bar and melt-sealed using the hydrogen-oxygen burner. Afterwards, annealing in the muffle furnace was done. The final temperature was 1123 K, and the ramp was 50 K/h. The annealing was done for 3 hours, and after that, rapid cooling was done using the melting ice. Generally, the procedure almost completely repeats the one used to obtain $\text{Li}_2\text{FeS}_{1-x}\text{Se}_x\text{O}$ series earlier^[13].

After grinding in an agate mortar, the materials appeared in the form of dark grey powders, if M – Fe, Co, and of brown shade, if Mn was present in the composition. The phase purity was checked by conducting powder X-ray diffraction using Stoe Stadi P (Germany) diffractometer, equipped with Mythen 1K detector (Dectris), in Debye-Scherrer geometry. The measurements were conducted in sealed glass capillaries (Mark tubes, Glass No. 14, Hilgenberg) with 0.3 mm

inner diameter. The radiation used was $\text{CoK}\alpha_1$, and the monochromator was Ge (111). Structural refinement by Rietveld method^[43]/profile fitting by Le Bail method^[44] were done using Jana2006 program^[45].

In situ Powder X-ray Diffraction Studies

A stoichiometric mixture of Li_2O , Fe, and Se was put into quartz capillary and sealed. Then, the following steps were done: the temperature was increased by 30 degrees and maintained constant for one minute to take a powder diffractogram using the synchrotron radiation. The experiment was carried out at P02.1 beamline at DESY^[46]. Temperature was controlled by a custom-made thermo-couple, which was calibrated beforehand. The heating was done using Oxford Hot-Air-Blower. The described sequence was repeated, until the reaction with quartz caused the destruction of the capillary.

The wavelength was 0.20733 Å, and the data was collected using Perkin Elmer XRD1621 CN3 – EHS 2D detector. For detector calibration, the LaB_6 standard was used. Data integration from the 2D detector was realized using the DAWN software^[47].

Electrode Preparation and Electrochemical Experiments

The electrodes were prepared by mixing the Li_2MSeO samples with carbon black (Super P) conductive additive and polytetrafluoroethylene (Sigma Aldrich) binder in the mass ratio of 8:1:1, using an agate mortar. The mixture was pressed onto aluminum mesh, applying the pressure of 2 tons/cm².

The measurements were performed using a thermostated VMP3 potentiostat (Biologic Instruments, France) at 298 K. The assembled electrochemical cells were of Swagelok® type. Glass fiber (Whatman, GF/D) which served as separator was soaked in the electrolyte (1M $\text{LiPF}_6/\text{EC}:\text{DEC}$, 3:7 by volume, Sigma Aldrich). Metallic lithium (99.9%, G-Materials) served as counter-electrode. For galvanostatic cycling with potential limitation, a voltage window between 1.2 and 3.0 V vs Li^+/Li was set, as in our previous works^[10-13]. For Li_2FeSeO , the lower cut-off was set to 0.8 V for the first series of electrochemical measurements at 0.1C, and for Li_2MnSeO it was set for 1.5 V, since these two materials showed significantly different electrochemical behaviour. This variation was done to achieve higher values of Coulombic efficiency. Rate capability evaluation was done for 10 cycles at 0.1C, 0.2C, 0.5C, 1C, and again at 0.1C. The C value, which was calculated using the Faraday's equation^[48], corresponds to the charge transferred by 1 Li-ion removed from the Li_2MSeO formula unit, thus 0.1C corresponds to current density required for the removal of 1 Li^+ within 10 hours. Typical galvanostatic charge/discharge curves for all six compositions are presented in Figure S4. For ensuring the data reliability, the measurements were repeated three times for each compound. As visible from the curves, introduction of manganese slightly increases the average cell operation voltage, as it does for sulfur-based anti-perovskites^[10-12].

Typical galvanostatic charge-discharge curves for all six compositions are presented in Figure S4. For ensuring the data reliability, the measurements were repeated three times for each compound. As visible from the curves, introduction of manganese slightly increases the average cell operation voltage, as it does for sulfur-based anti-perovskites^[10-12].

Operando X-ray Diffraction

Operando measurements were conducted at two different beamlines: P02.1 (DESY, Hamburg)^[46] and BL04-MSPD (ALBA, Barcelona)^[49]. The same detector was used for *operando* XRD studies at P02.1, as the one for *in situ*, and at BL04-MSPD, the High-throughput Position Sensitive Detector MYTHEN (Dectris/PSI Detectors group) was used for data collection. The wavelengths at these two beamlines were different (0.20741 Å at P02.1 and 0.4127 Å at BL04-MSPD), thus the data in the article is presented with $Q = 4\pi\sin(\theta)/\lambda$ on the x-axis, for the same reflections selected.

Electrodes were prepared in the same manner as for electrochemical tests, the only difference was in the mesh: for operando studies, the aluminum mesh with bigger cell was used, to minimize contribution of aluminum in diffractograms. The electrochemical cells were of a coin-type, with custom-made modification, representing the holes in their housing, covered by glass.

A special 8-fold rotating sample holder, designed for *operando* electrochemical experiments^[50] connected to a VMP3 potentiostat (Biologic Instruments, France) was applied.

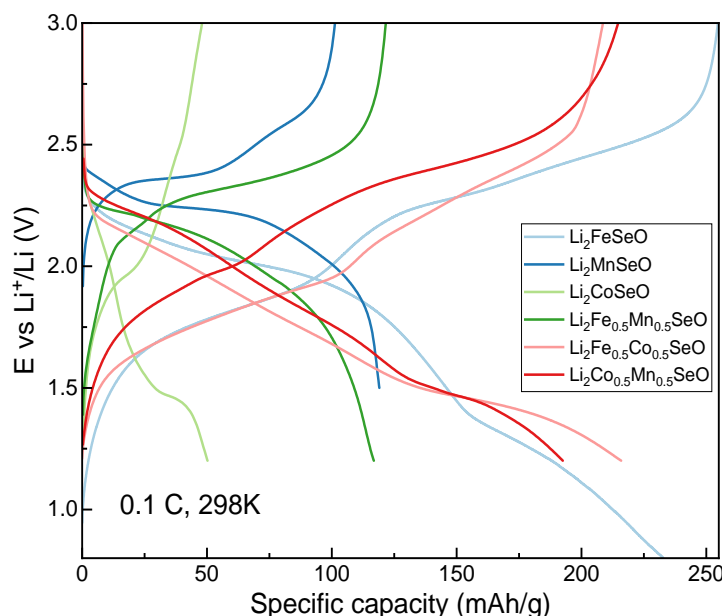


Figure S4. Typical galvanostatic charge-discharge curves for six Li_2MSeO compositions.

The cells were charged and discharged at a 0.1C current density, and the acquisition time was 1 minute for diffractogram. Including the holder rotation and application of the script commands to the equipment, it was possible to obtain one diffraction pattern every 10 minutes for each sample. The data collection protocol used was the same at both XRD beamlines. The 2θ range was 0 – 20 degrees at P02.1, and 0 – 40 degrees at BL04-MSPD. The range of 0 – 1.5 degrees was covered by the beam stops, and thus not accounted for the profile analysis.

Operando X-ray Absorption Spectroscopy (XAS)

XAS experiments were also conducted at two different beamlines with similar functionality^[51-52]. Monochromator crystal was Si (111). Energy calibration was done using the foils made out of elements of interest. The data was collected in both transmission and fluorescence yield modes, and the processing and analysis were done using the Demeter software pack^[53]. Ionization chambers filled with a single gas or a gas mixture, depending on the photon energy, served as detectors, except for the fluorescence, for which the special Si-PIPS detector was used.

The electrodes were prepared as for operando XRD, but the windows of the coin cells were made out of Kapton, to reduce the loss of photons before and after the sample. Electrochemical part was absolutely the same as for operando XRD, as well as the 8-fold sample holder. The energy range of 150 eV before and 800 eV after the K-edge of the element was recorded for fine structure calculations. Note that sometimes, like for $\text{Li}_2\text{Fe}_{0.5}\text{Mn}_{0.5}\text{SeO}$, the XAFS area is reduced for Mn K-edge, as it lays quite close to the Fe K-edge on the energy grid. One measurement took between 3 and 4 minutes, allowing to obtain 1 spectrum for a sample within about 35 – 50 minutes, including all the necessary adjustments of the beamline equipment.

Compositions with defined oxidation state for the element of interest were used as standards. Calibration lines for the oxidation states of transition metals were built using the following materials: MnO, Mn_2O_3 and MnO_2 for Mn K-edge; FeO, Fe_3O_4 and Fe_2O_3 for Fe K-edge; CoO, Co_3O_4 and Co(III) acetylacetonate for Co K-edge. To collect the spectra, the materials were mixed with carboxymethylcellulose in the mass ratio of 1:3 and a total mass of 40 mg, then pressed into pellets of 13 mm diameter. The lines are presented in Figure S5.

For Co K-edge, the calibration is not shown, as cobalt remained inactive in all the materials. As shown in the main text, we attempted to use Se and FeSe as standards for selenium in corresponding oxidation state, but the relation of this parameter and the edge energy is more complicated in this case than for 3d metals. Note that initial positions of the edge energies were defined from the first energy derivatives.

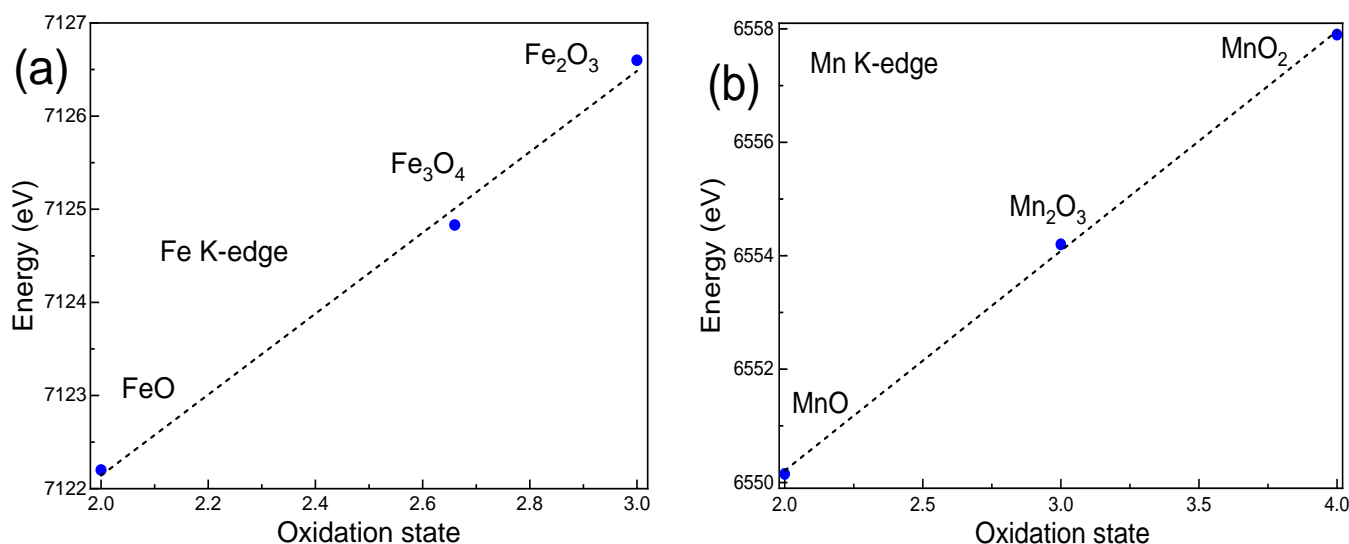


Figure S5. Calibration lines for evaluating the oxidation states of (a) iron and (b) manganese in Li_2MSeO anti-perovskites from the X-ray absorption spectroscopy.

Supplementary Data

Figure S6 demonstrates the contour-plots of *operando* X-ray diffractograms obtained during charge and discharge of $\text{Li}_2\text{Co}_{0.5}\text{Mn}_{0.5}\text{SeO}$ (panel a), and the comparison between $\text{Li}_2\text{Co}_{0.5}\text{Mn}_{0.5}\text{SeO}$ and $\text{Li}_2\text{Fe}_{0.5}\text{Mn}_{0.5}\text{SeO}$ at selected states of charge (panels b and c).

In Figures S7 – S10, the results of *operando* XAS studies for Li_2MnSeO , Li_2CoSeO , $\text{Li}_2\text{Fe}_{0.5}\text{Co}_{0.5}\text{SeO}$, $\text{Li}_2\text{Fe}_{0.5}\text{Mn}_{0.5}\text{SeO}$ and $\text{Li}_2\text{Co}_{0.5}\text{Mn}_{0.5}\text{SeO}$ are presented.

For Li_2MnSeO (Figure S7a), a noticeable electrochemical activity of manganese (Figure S4a) and selenium

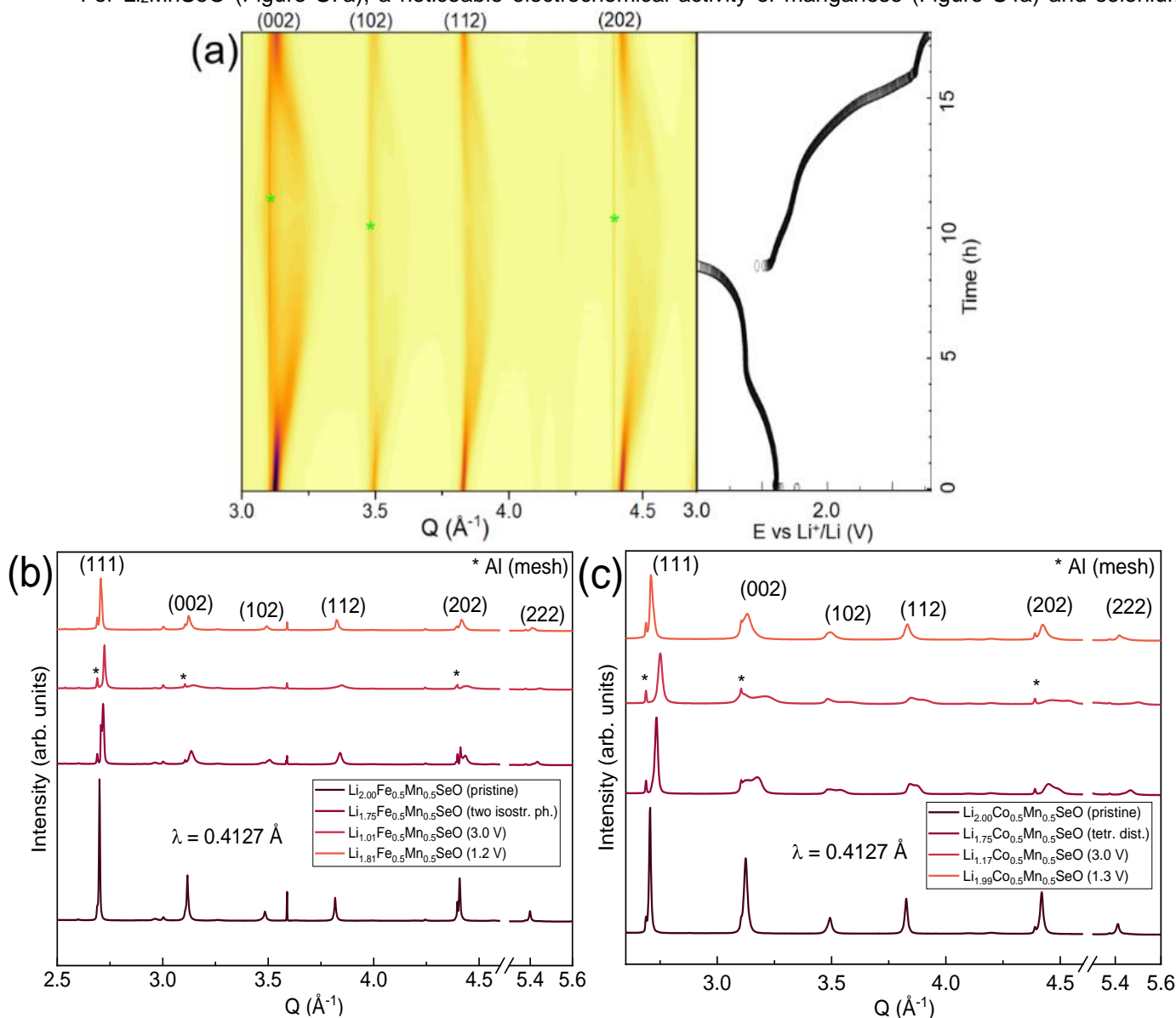


Figure S6. (a) – contour-plots of *operando* XRD and corresponding galvanostatic curve for $\text{Li}_2\text{Co}_{0.5}\text{Mn}_{0.5}\text{SeO}$, (b-c) – comparative analysis of selected reflections for $\text{Li}_2\text{Fe}_{0.5}\text{Mn}_{0.5}\text{SeO}$ and $\text{Li}_2\text{Co}_{0.5}\text{Mn}_{0.5}\text{SeO}$.

(Figure S7b and Figure S7c) was observed. The redox activity of Mn is reversible, and the Mn-based redox process is dominant for this compound. The redox activity of Se is less reversible.

In contrast, in Li_2CoSeO , the cationic oxidation is close to zero, and charge compensation is based on the electroche Figure S9 shows the redox behaviour of Fe, Co and Se in $\text{Li}_2\text{Fe}_{0.5}\text{Co}_{0.5}\text{SeO}$. An enhanced electrochemical activity of Se compared to pure iron compound Li_2FeSeO can be concluded. The Fe-cations are redox-active while the Co cations inactive. The $\text{Li}_2\text{Fe}_{0.5}\text{Co}_{0.5}\text{SeO}$ composition is the best example for the “boosting” effect of cobalt presence in the structure. mical activity of Se (Figure S8a and b). The redox activity of Se in this compound is reversible.

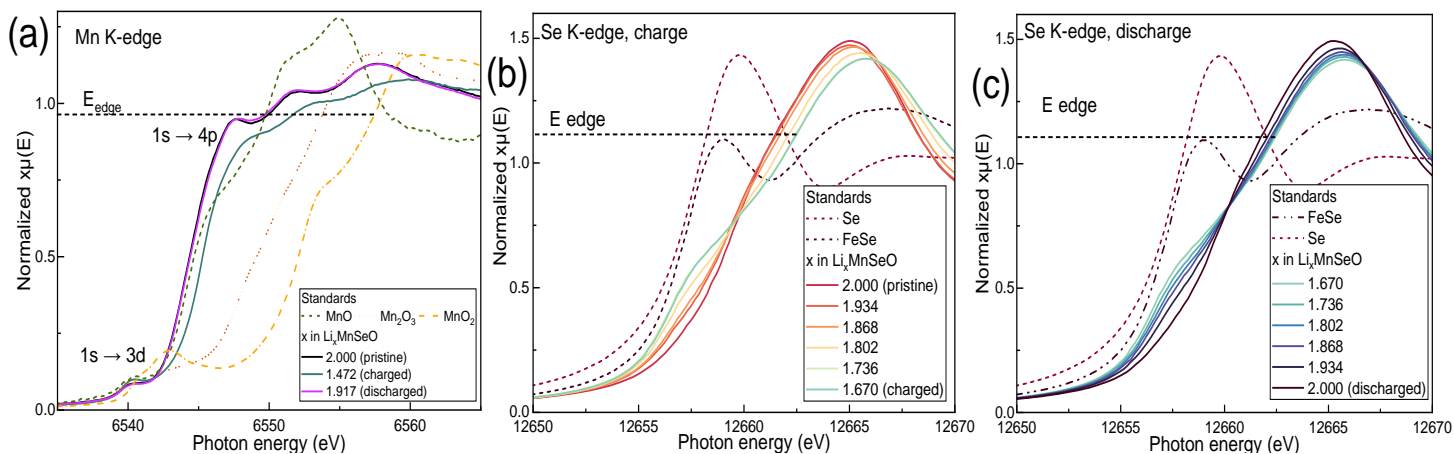


Figure S7. Operando XAS of Li_2MnSeO . (a) – Mn K-edge region in pristine, charged and discharged states, (b – c) – Se K-edge on charge and discharge.

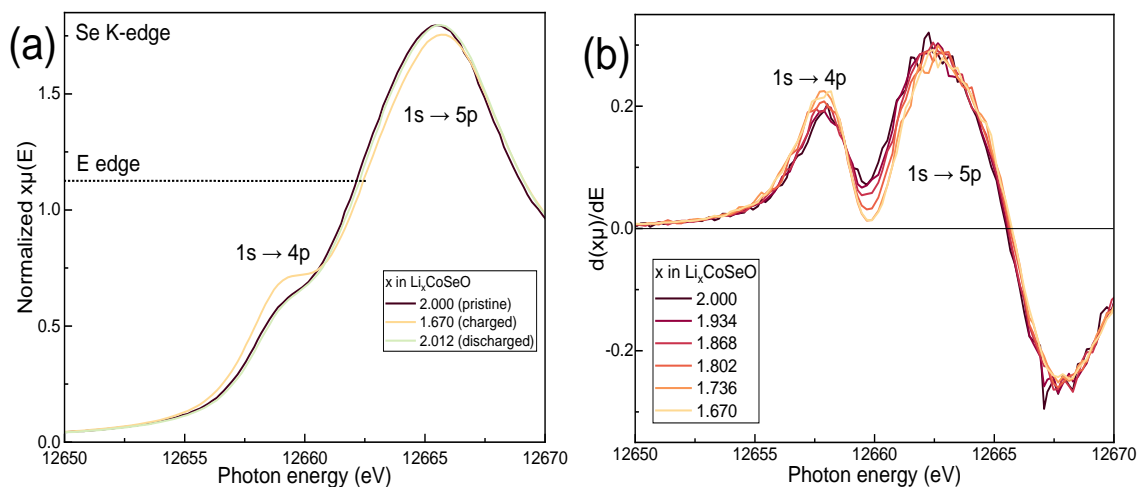


Figure S8. Operando XAS of Li_2CoSeO . (a) – Se K-edge of the material in pristine, charged and discharged states, (b) – first energy derivative of the normalized spectra during charge.

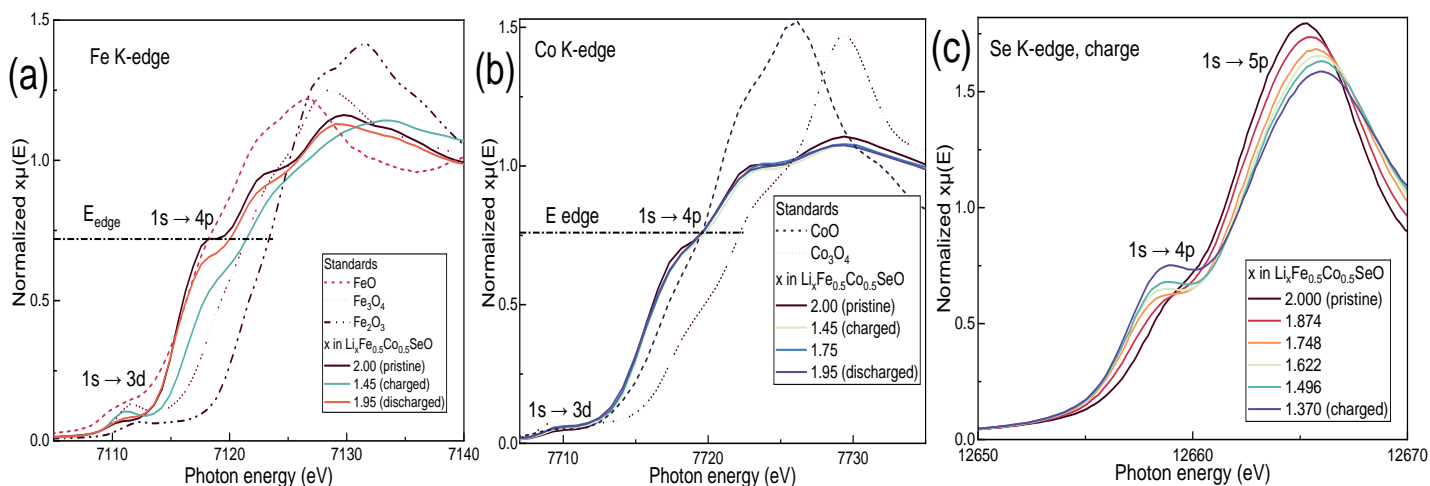


Figure S9. Operando XAS of $\text{Li}_2\text{Fe}_{0.5}\text{Co}_{0.5}\text{SeO}$. (a - b) – Fe and Co K-edge, respectively, for the pristine, charged and discharged states, (c) – Se K-edge during charge.

Figure S10 illustrates the redox behaviour of Fe, Mn and Se in $\text{Li}_2\text{Fe}_{0.5}\text{Mn}_{0.5}\text{SeO}$. All the three elements are electrochemically active in this compound. On the cationic site, the activity of Fe is higher than of Mn.

Figure S11 confirms the “boosting” effect of cobalt in $\text{Li}_2\text{Co}_{0.5}\text{Mn}_{0.5}\text{SeO}$. Here, Mn (panel a) and Se (panel b) are redox-active while Co is non-active (data not shown).

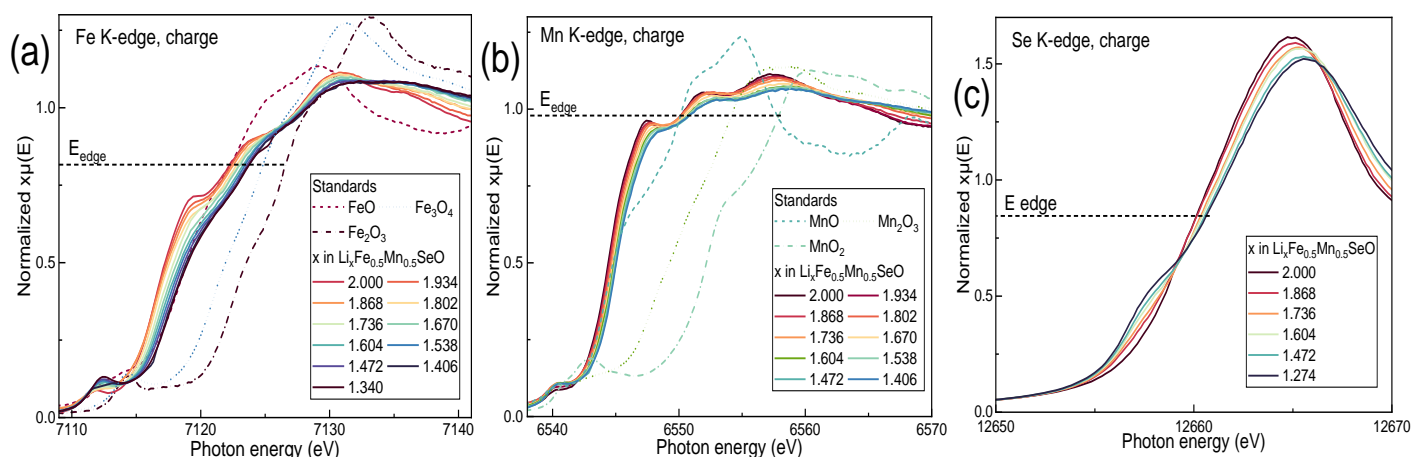


Figure S10. Operando XAS of $\text{Li}_2\text{Fe}_{0.5}\text{Mn}_{0.5}\text{SeO}$. (a) – Fe K-edge, (b) – Mn K-edge, (c) – Se K-edge during charge.

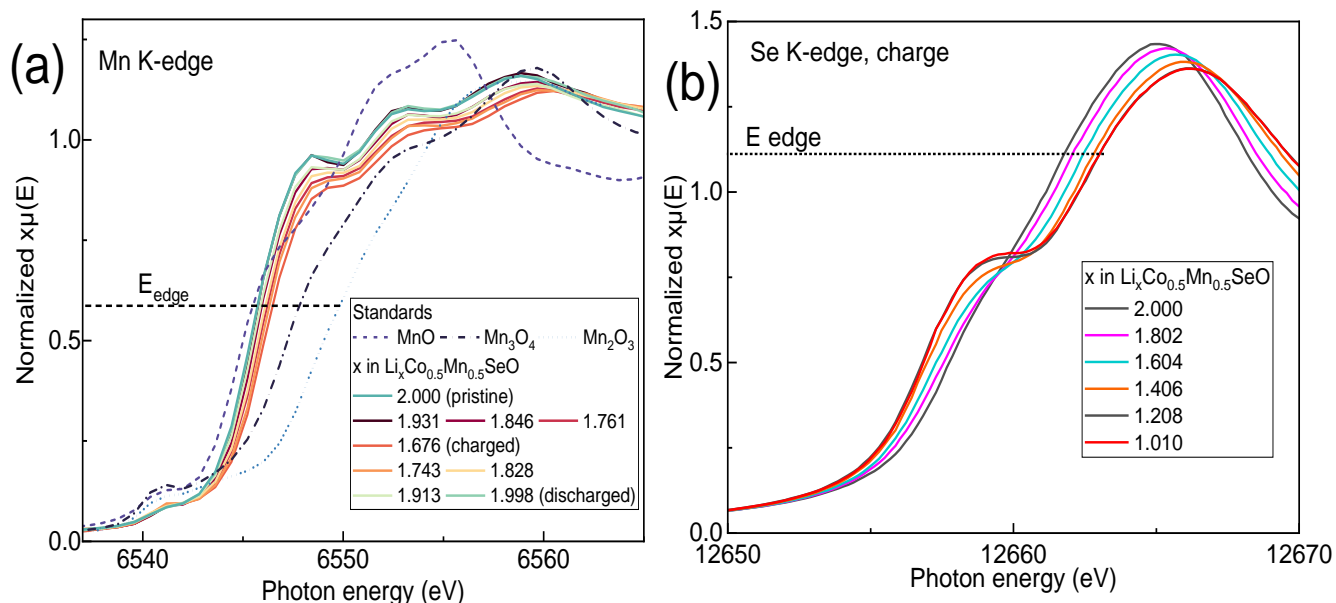


Figure S11. Operando XAS of $\text{Li}_2\text{Co}_{0.5}\text{Mn}_{0.5}\text{SeO}$. (a) – Mn K-edge during charge and discharge, (b) – Se K-edge during charge.

Results of the EXAFS analysis for Fe-Kedge and Se K-edge spectra of Li_2FeSeO in different states of charge are shown in Figure S12. The k^3 -weighted and Fourier-transformed XAFS functions for Fe in pristine, charged and discharged states are shown in panels a-c, while for Se in panels d-f.

The analysis confirms a significant local structural distortion in the first two coordination shells of iron and selenium. In particular, the distances between Se and Fe, and between Fe and Se change drastically, pointing to a break of the chemical bonds in Li_2FeSeO with formation of FeSe and/or elemental Se. This statement agrees with the structural collapse observed in *operando* XRD data. The fitting of the XAFS functions of Fe and Se for the discharged state of Li_2FeSeO includes FeSe and Se.

Table S13 shows local structural information (distances in the first two coordination shells of corresponding absorbing ions) for the five Li_2MSeO compounds.

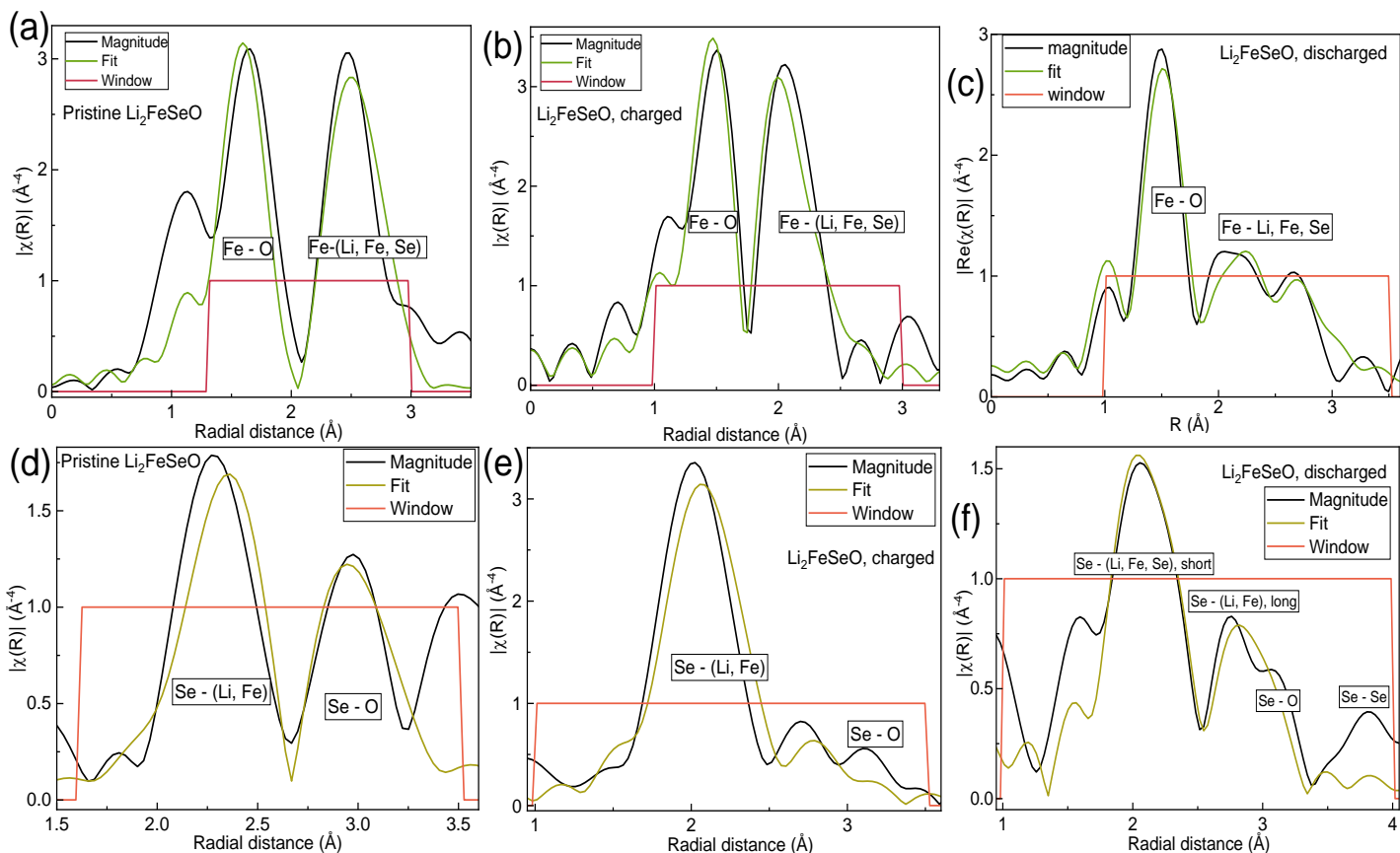


Figure S12. XAFS fitting of Li_2FeSeO in the pristine, charged and discharged states: (a – c) from Fe K-edge, (d – f) – from Se K-edge.

Table S13. XAFS data for $\text{Li}_x\text{Fe}_{0.5}\text{Co}_{0.5}\text{SeO}$, Li_xMnSeO , Li_xCoSeO , $\text{Li}_x\text{Co}_{0.5}\text{Mn}_{0.5}\text{SeO}$ and $\text{Li}_x\text{Fe}_{0.5}\text{Mn}_{0.5}\text{SeO}$.

x in $\text{Li}_x\text{Fe}_{0.5}\text{Co}_{0.5}\text{SeO}$	Fe – O distance, Å	Fe – (Li, Fe, Co, Se) distance, Å
2.00 (pristine)	1.99 ± 0.01	2.86 ± 0.01
0.77 (charged)	Insufficient data quality	
1.98 (discharged)		
	Se – (Li, Fe, Co) distance, Å	Se – O distance, Å
2.00 (pristine)	2.75 ± 0.08	3.41 ± 0.02
1.37 (charged)	2.47 ± 0.03	3.34 ± 0.02
1.99 (discharged)	2.77 ± 0.02	3.44 ± 0.02
x in Li_xMnSeO	Se – (Li, Mn) distance, Å	Se – O distance, Å
2.00 (pristine)	2.89 ± 0.03	3.60 ± 0.02
1.67 (charged)	2.58 ± 0.01	Insufficient data quality
2.07 (discharged)	2.91 ± 0.02	3.62 ± 0.02
x in Li_xCoSeO	Se – (Li, Co) distance, Å	Se – O distance, Å
2.00 (pristine)	2.75 ± 0.07	3.43 ± 0.02
1.65 (charged)	2.75 ± 0.01	3.41 ± 0.01
1.99 (discharged)	2.75 ± 0.01	3.43 ± 0.01
x in $\text{Li}_x\text{Co}_{0.5}\text{Mn}_{0.5}\text{SeO}$	Se – (Li, Co, Mn) distance, Å	Se – O distance, Å
2.00 (pristine)	2.79 ± 0.01	3.47 ± 0.02
1.01 (charged)	2.53 ± 0.02	Insufficient data quality
1.984 (discharged)	2.77 ± 0.03	3.48 ± 0.02
x in $\text{Li}_x\text{Fe}_{0.5}\text{Mn}_{0.5}\text{SeO}$	Se – (Li, Fe, Mn) distance, Å	Se – O distance, Å
2.00 (pristine)	2.82 ± 0.02	3.49 ± 0.09
1.274 (charged)	Insufficient data quality	
1.99 (discharged)	2.86 ± 0.02	3.50 ± 0.07